Figures and figure supplements

High-endothelial cell-derived S1P regulates dendritic cell localization and vascular integrity in the lymph node

Szandor Simmons *et al*

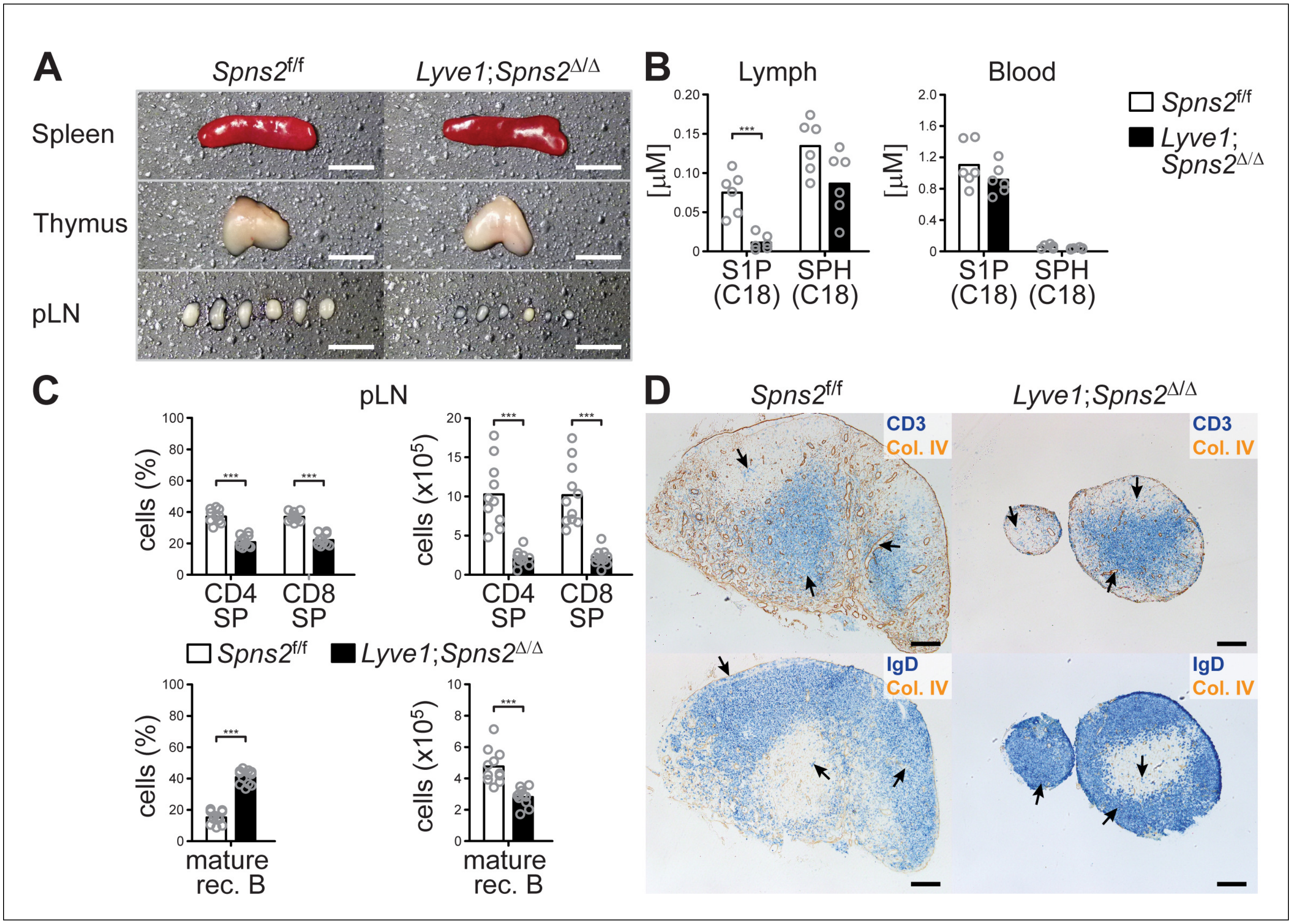

Figure 1. *Lyve1*^{CRE}-mediated *Spns2*-deletion in endothelial cells causes hypotrophy in pLNs. (**A**) Macroscopic view of spleen, thymus and pLNs of wildtype *Spns2*$^{f/f}$ (left) and *Lyve1;Spns2*$^{\Delta/\Delta}$ (right) mice. (**B**) Quantification of S1P and sphingosine (SPH) concentrations in lymph and blood. (**C**) FACS analysis of CD4^{+} and CD8^{+} SP T-cells (top) and mature rec. B-cells (bottom) of pLNs of *Spns2*$^{f/f}$ and *Lyve1;Spns2*$^{\Delta/\Delta}$ mice. (**D**) Light microscopy of pLNs of *Spns2*$^{f/f}$ (left) and *Lyve1;Spns2*$^{\Delta/\Delta}$ (right) mice for CD3^{+} T-cells (top, blue) and IgD^{+} mature rec. B-cells (bottom, blue) counterstained for collagen-IV^{+} (brown) tissue frameworks. Each circle (**B, C**) represents an individual mouse; bars indicate the mean. Scale bars, 0.2 cm (**A**) or 200 µm (**D**). ***$p<0.0005$ (two-tailed unpaired Student's *t*-test (**B, C**)). Data are representative for six mice per group (**A, B**), for 2x inguinal, 2x brachial and 2x axial LNs of six mice per group (**D**) or are pooled from three independent experiments (**C**) with n = 3 or n = 4 mice per group.

DOI: https://doi.org/10.7554/eLife.41239.002

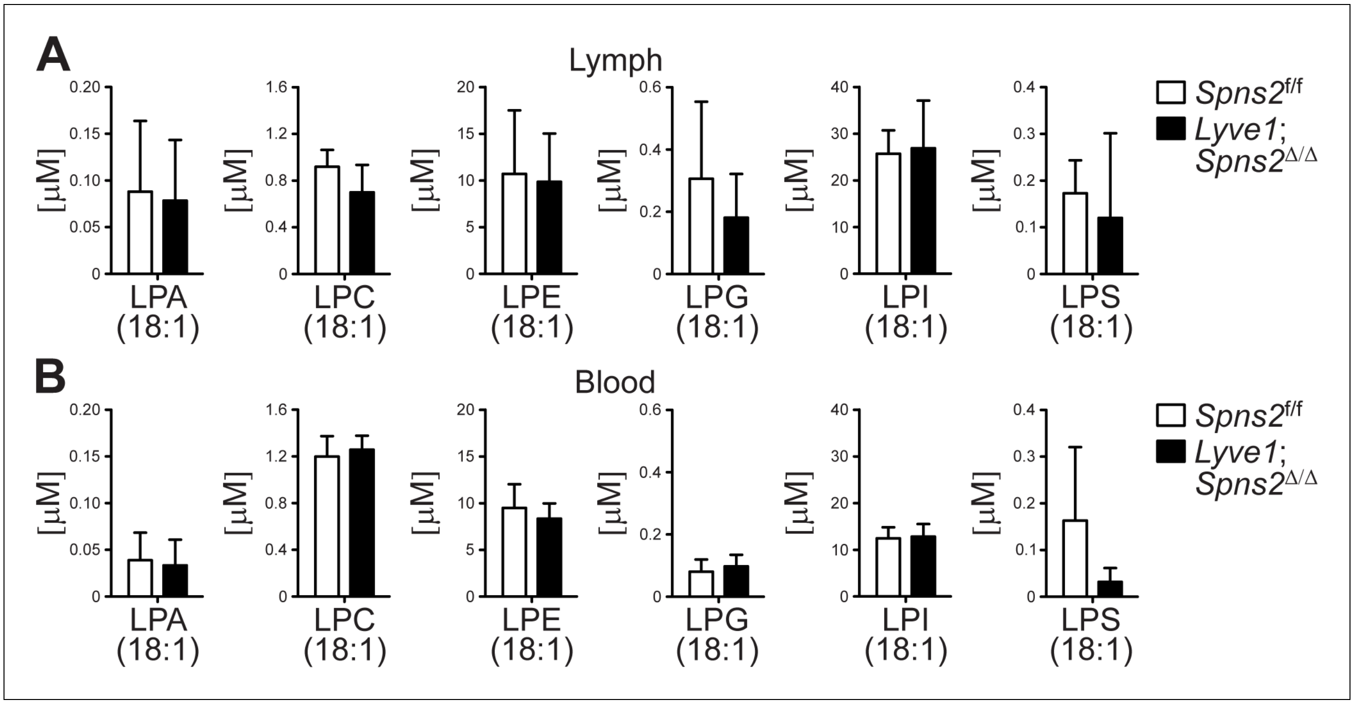

Figure 1—figure supplement 1. *Lyve1*CRE mediated *Spns2*-deficiency does not affect glycerol-based lysophospholipid levels, representatively shown for C18:1 species (other species (not shown) were also checked and found to be not different), in lymph and blood. (**A**) Quantification of lymph concentrations of lysophosphatidic acid (LPA), lysophosphatidylcholine (LPC), lysophosphatidyethanolamine (LPE), lysophosphatidyglycerol (LPG), lysophosphatidylinositol (LPI) and lysophosphatidylserine (LPS). (**B**) Blood concentrations of glycerol-based lysophospholipids (as monitored in (**A**)). Data are representative for six mice per group (**A**), (**B**); mean + s.e.m. in A, (**B**).

DOI: https://doi.org/10.7554/eLife.41239.003

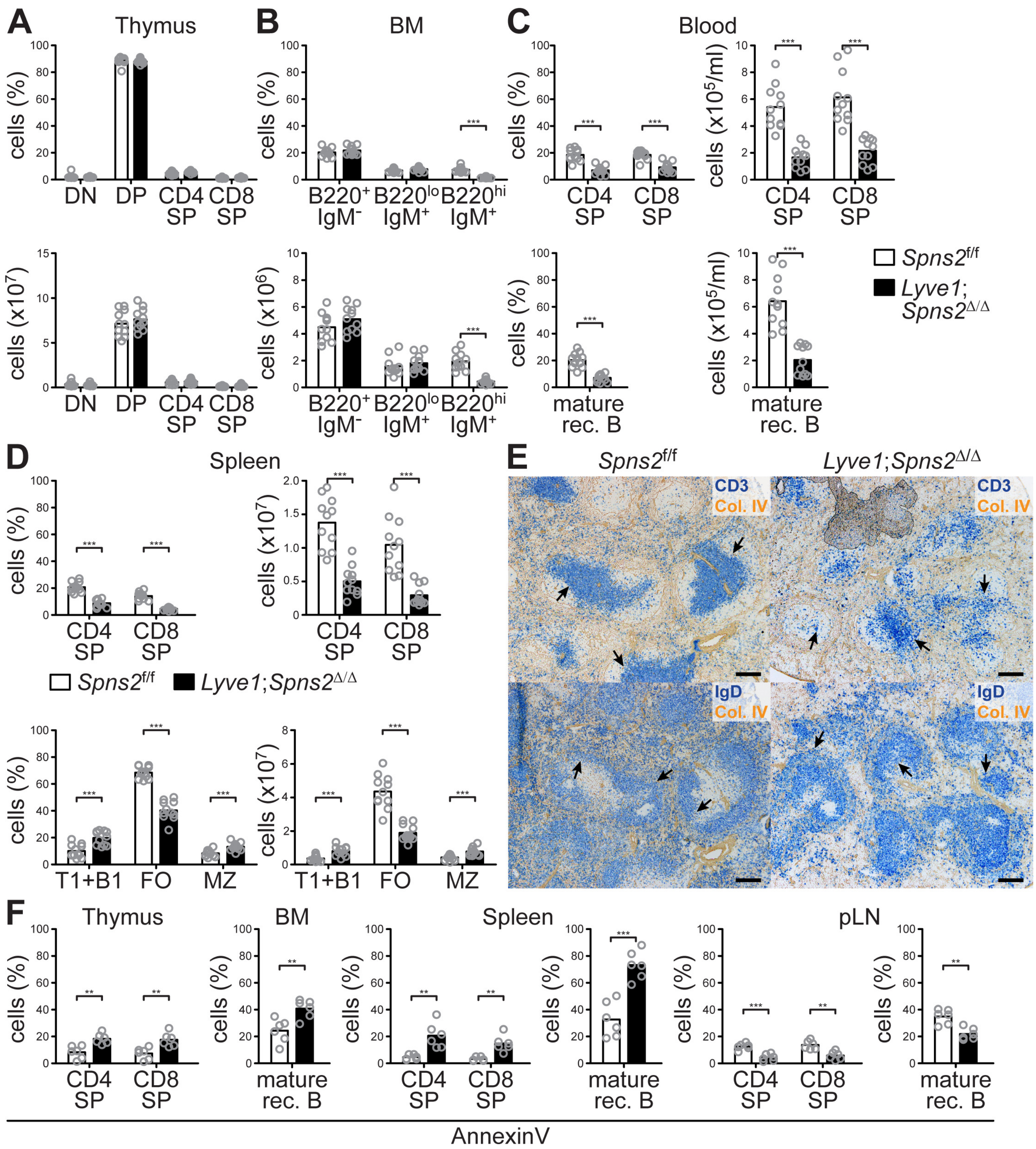

Figure 1—figure supplement 2. Recirculating lymphocyte populations are impaired throughout various lymphatic tissues in *Lyve1;Spns2*$^{\Delta/\Delta}$ mice. (**A**) FACS analysis of thymocytes and T-cells in the thymus of *Spns2*$^{f/f}$ and *Lyve1;Spns2*$^{\Delta/\Delta}$ mice. (**B**) FACS analysis of precursor B-cells (B220^{+}/IgM^{-}), immature B-cells (B220^{lo}/IgM^{+}) and mature rec. B-cells (B220^{hi}/IgM^{+}) in the BM of *Spns2*$^{f/f}$ and *Lyve1;Spns2*$^{\Delta/\Delta}$ mice. (**C**) FACS analysis of CD4^{+} and CD8^{+} SP T-cells (top) and mature rec. B-cells (bottom) in the blood of *Spns2*$^{f/f}$ and *Lyve1;Spns2*$^{\Delta/\Delta}$ mice. (**D**) FACS analysis of CD4^{+} and CD8^{+} SP T-cells

Figure 1—figure supplement 2 continued on next page

Figure 1—figure supplement 2 continued

(top) and B220^{+}/CD21^{-}/CD23^{-} transitional (**T1**) and B1 B-cells (bottom), B220^{+}/CD21^{+}/CD23^{+} follicular (FO) B-cells (bottom) and B220^{+}/CD21^{hi}/CD23^{lo}marginal zone (MZ) B-cells (bottom) in the spleen of *Spns2*$^{f/f}$ and *Lyve1;Spns2*$^{\Delta/\Delta}$ mice. (**E**) Light microscopy of the spleen of *Spns2*$^{f/f}$ (left) and *Lyve1;Spns2*$^{\Delta/\Delta}$ (right) mice for CD3^{+} T-cells (top, blue) and IgD^{+} mature rec. B-cells (bottom, blue) counterstained for collagen-IV^{+} (brown) tissue frameworks. (**F**) FACS analysis of apoptotic CD4^{+} and CD8^{+} SP T-cells (left) and mature rec. B-cells (right) by AnnexinV-staining in the thymus, BM, spleen and pLNs of *Spns2*$^{f/f}$ and *Lyve1;Spns2*$^{\Delta/\Delta}$ mice. Each circle (**A–C, D, F**) represents an individual mouse; bars indicate the mean. Scale bars, 200 µm (**E**). *p<0.05; **p<0.005; ***p<0.0005 (two-tailed unpaired Student's *t*-test (**A–C, D, F**)). Data are pooled from three independent experiments (**A–D, D, F**) with n = 3 or n = 4 mice per group (**A–C, D, F**), or are representative for six mice per group (**E**).

DOI: https://doi.org/10.7554/eLife.41239.004

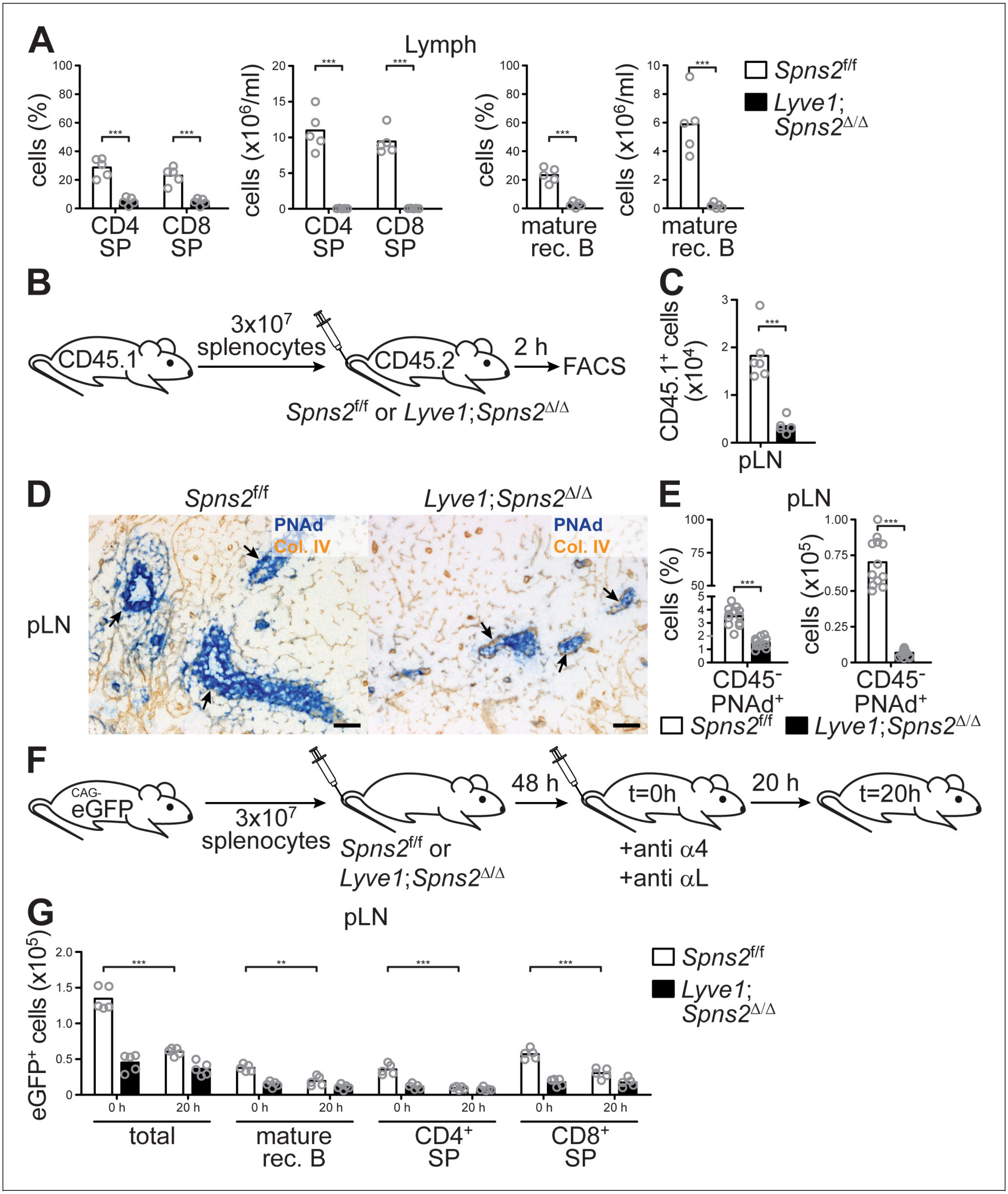

Figure 2. The immigration of lymphocytes into pLNs and their egress into the lymphatic system is severely impaired in Lyve1;*Spns2*$^{\Delta/\Delta}$ mice. (**A**) FACS analysis of CD4$^+$ and CD8$^+$ SP T-cells (left) and mature rec. B-cells (right) of lymph fluid isolated from the *cisterna chyli* of *Spns2*$^{f/f}$ and *Lyve1;Spns2*$^{\Delta/\Delta}$ mice. (**B**) Experimental flow-chart of short-terming homing assays to quantify lymphocyte immigration into pLNs. (**C**) FACS analysis of total congenic

Figure 2 continued on next page

Figure 2 continued

CD45.1$^+$ cells in pLNs two hours upon injection of WT splenocytes into *Spns2*$^{f/f}$ and *Lyve1;Spns2*$^{\Delta/\Delta}$ mice. (**D**) Light microscopy of frozen sections of pLNs of *Spns2*$^{f/f}$ (left) and *Lyve1;Spns2*$^{\Delta/\Delta}$ (right) mice for PNAd$^+$ HEVs (blue) counterstained for collagen-IV$^+$ (brown). (**E**) FACS analysis of total CD45$^-$/CD31$^+$/PNAd$^+$ high-endothelial cells isolated from pLNs of *Spns2*$^{f/f}$ and *Lyve1;Spns2*$^{\Delta/\Delta}$ mice. (**F**) Experimental flow-chart of homing assays to quantify lymphocyte egress from pLNs. (**G**) Total numbers of congenic eGFP$^+$ cells in pLNs at 0 hr and 20 hr upon injection of anti-α_4 / anti-α_L antibodies into *Spns2*$^{f/f}$ and *Lyve1;Spns2*$^{\Delta/\Delta}$ mice. Each circle (**A, C, E, G**) represents an individual mouse; bars indicate the mean. Scale bars, 50 μm (**D**). **p<0.005; ***p<0.0005 (two-tailed unpaired Student's *t*-test (**A, C, E, G**)). Data are representative for five mice per group pooled from two independent experiments (**A**) with n = 2 or n = 3 mice per group (**A**), for six mice per group (**D**) or are pooled from two (**C, G**) or three (**E**) independent experiments with n = 2, n = 3 or n = 4 mice per group.

DOI: https://doi.org/10.7554/eLife.41239.005

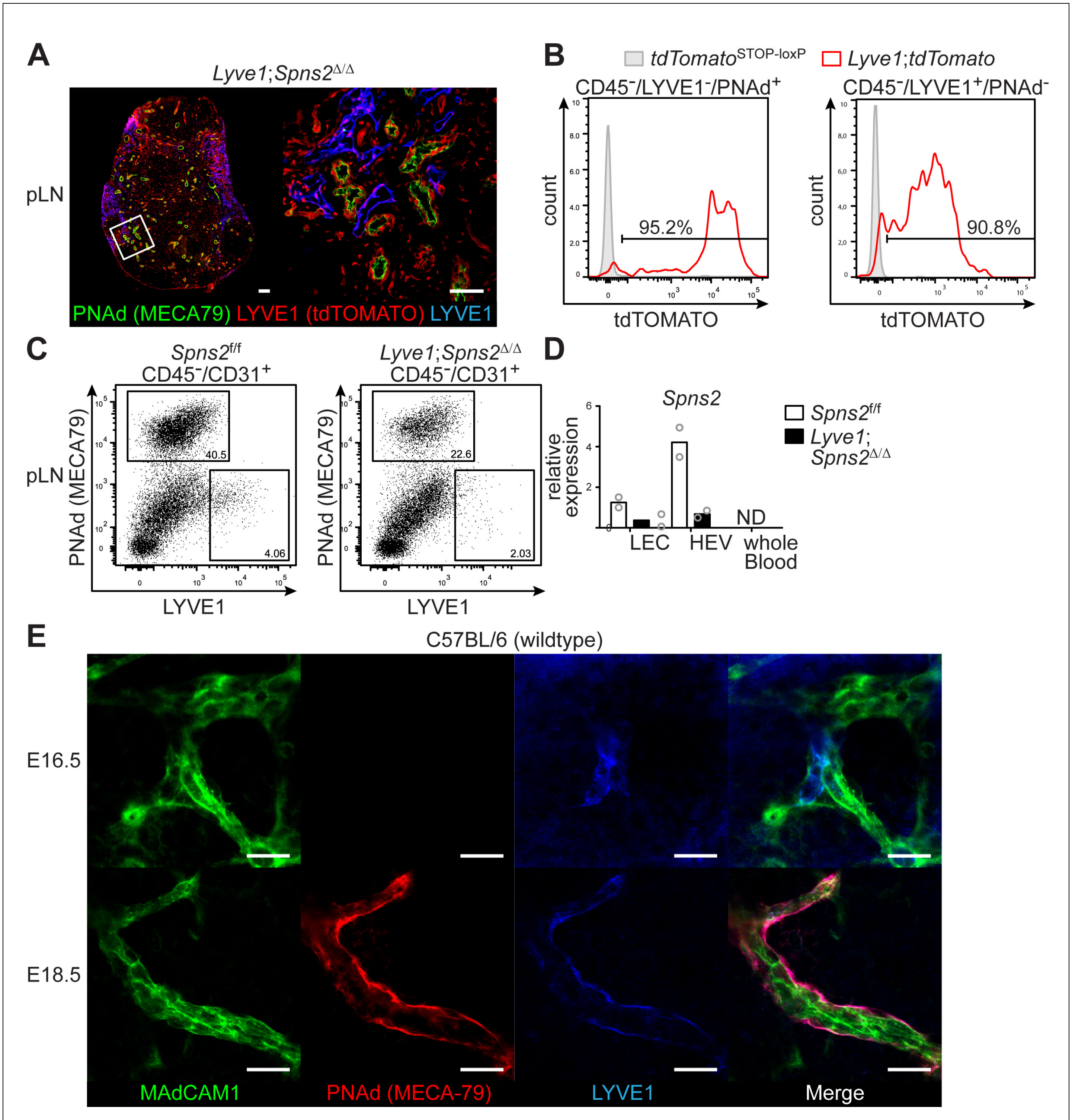

Figure 2—figure supplement 1. *Spns2* is effectively deleted in LECs and HEVs of *Lyve1;Spns2*$^{\Delta/\Delta}$ mice. (**A**) Confocal microscopy of pLNs of *Lyve1; tdTomato* reporter mice for tdTOMATO^{+} (LYVE1^{-}) expressing cells (red), PNAd^{+} (green) HEVs and Lyve-1^{+} (blue) LECs. (**B**) FACS analysis of CD45^{-}/CD31^{+}/PNAd^{+}/Lyve-1^{-} high-endothelial cells and CD45^{-}/CD31^{+}/PNAd^{-}/Lyve-1^{+} LECs isolated from pLNs of *tdTomato*$^{\text{STOP-loxP}}$ control mice or *Lyve1; tdTomato* mice for tdTOMATO expression. (**C**) FACS analysis of CD45^{-}/CD31^{+}/PNAd^{+}/Lyve-1^{-} high-endothelial cells and CD45^{-}/CD31^{+}/PNAd^{-}/Lyve-1^{+} LECs of pLNs of *Spns2*$^{f/f}$ and *Lyve1;Spns2*$^{\Delta/\Delta}$ mice. (**D**) Quantitative RT-PCR analysis of *Spns2* mRNA in sorted LECs, HEVs (as in **C**) and of whole blood from *Spns2*$^{f/f}$ and *Lyve1;Spns2*$^{\Delta/\Delta}$ mice. (**E**) Confocal microscopy of whole mounts of iLNs isolated from embryos of E16.5 (top) and E18.5 (bottom) of WT C57BL/6 mice for MAdCAM-1 (green), PNAd (red) and Lyve-1 (blue) on high-endothelial cell progenitors and HEVs. Scale bars, 200 μm (A, left), 50

Figure 2—figure supplement 1 continued on next page

Figure 2—figure supplement 1 continued

μm (A, right) and 20 μm (**D**). Data are representative for three mice per group (**A**), or are representative for two individual experiments (**B–D**) of pooled non-hematopoietic cells from 2x pLNs, 2x iLNs, 2x aLNs, 2x bLNs, 6x cervical LNs collected from five mice per group (**B–D**), or are representative for five analyzed embryos per group (**E**).

DOI: https://doi.org/10.7554/eLife.41239.006

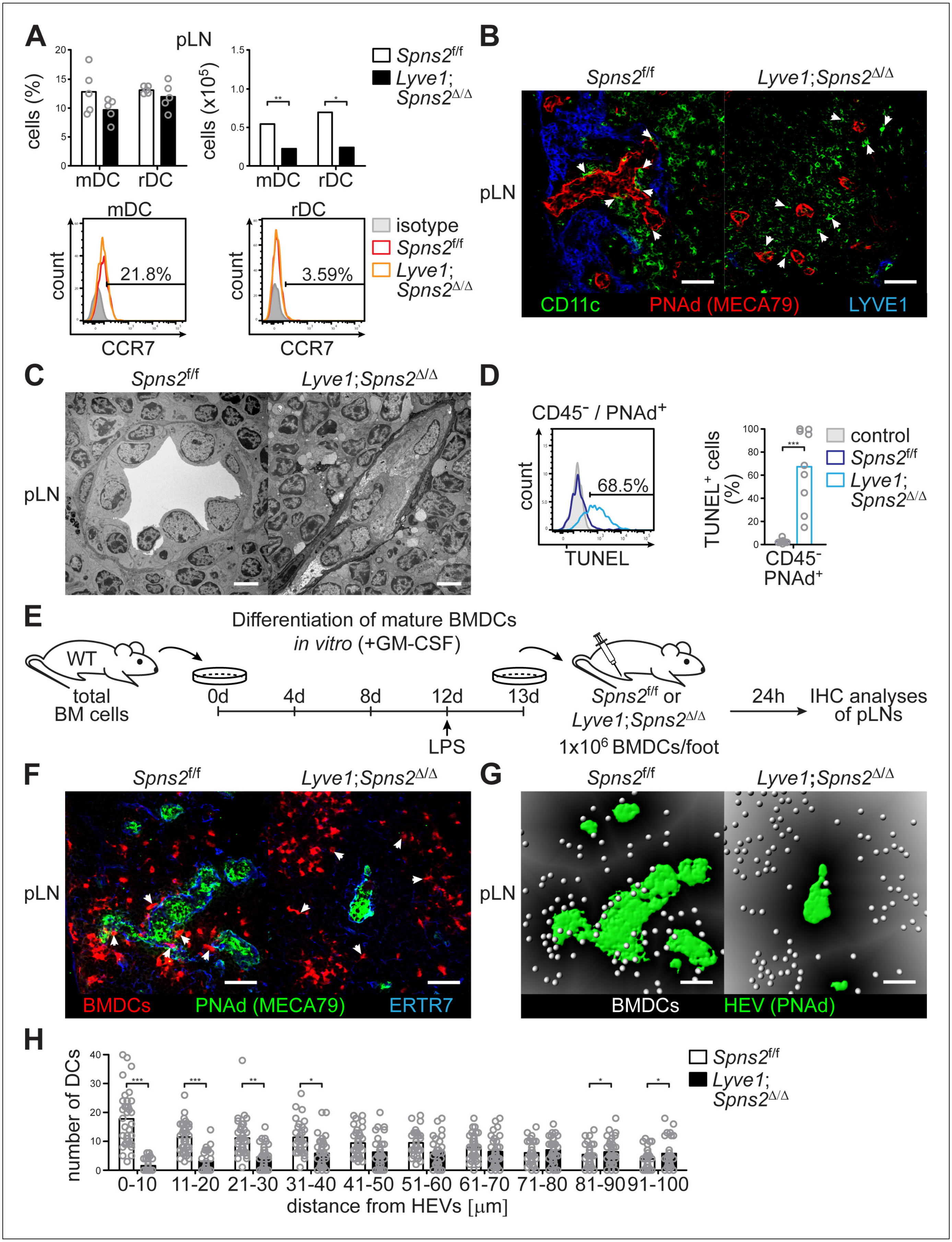
A
pLN
cells (%)
mDC rDC
cells (x10^5)
Spns2f/f
Lyve1; Spns2Δ/Δ
mDC
rDC
count
21.8%
3.59%
CCR7
isotype
Spns2f/f
Lyve1; Spns2Δ/Δ
B
Spns2f/f
Lyve1;Spns2Δ/Δ
pLN
CD11c
PNAd (MECA79)
LYVE1
C
Spns2f/f
Lyve1;Spns2Δ/Δ
pLN
D
CD45- / PNAd+
count
68.5%
TUNEL
TUNEL+ cells (%)
control
Spns2f/f
Lyve1; Spns2Δ/Δ
CD45- PNAd+
E
Differentiation of mature BMDCs in vitro (+GM-CSF)
WT
total BM cells
0d
4d
8d
12d
13d
LPS
Spns2f/f or Lyve1;Spns2Δ/Δ
1x10^6 BMDCs/foot
24h
IHC analyses of pLNs
F
Spns2f/f
Lyve1;Spns2Δ/Δ
pLN
BMDCs
PNAd (MECA79)
ERTR7
G
Spns2f/f
Lyve1;Spns2Δ/Δ
pLN
BMDCs
HEV (PNAd)
H
number of DCs
0-10
11-20
21-30
31-40
41-50
51-60
61-70
71-80
81-90
91-100
distance from HEVs [μm]
Spns2f/f
Lyve1; Spns2Δ/Δ

Figure 3. SPNS2-derived S1P controls interactions of PNAd$^+$ HEVs with lymph-derived dendritic cells in pLNs. (**A**) FACS analysis of CCR7-expression on endogenous conventional mDCs (CD3$^-$/CD19$^-$/CD11c^{int}/MHC-II^{hi}) and rDCs (CD3$^-$/CD19$^-$/CD11c^{hi}/MHC-II^{int}) isolated from pLNs of *Spns2*$^{f/f}$ and *Lyve1; Spns2*$^{\Delta/\Delta}$ mice. (**B**) Confocal microscopy of pLNs of *Spns2*$^{f/f}$ (left) and *Lyve1;Spns2*$^{\Delta/\Delta}$ (right) mice for CD11c$^+$ (green) DCs, PNAd$^+$ (red) HEVs and Lyve-1$^+$ (blue) LECs. (**C**) TEM images of HEVs in pLNs of *Spns2*$^{f/f}$ and *Lyve1;Spns2*$^{\Delta/\Delta}$ mice. (**D**) Flow-cytometric TUNEL assay on CD45$^-$/CD31$^+$/PNAd$^+$ high-endothelial cells isolated from pLNs of *Spns2*$^{f/f}$ and *Lyve1;Spns2*$^{\Delta/\Delta}$ mice. (**E**) Experimental flow-chart of BMDC-differentiation in vitro, and lymphatic homing assays of footpad injected BMDCs to quantify DC-immigration from afferent lymphatics into pLNs of *Spns2*$^{f/f}$ and *Lyve1;Spns2*$^{\Delta/\Delta}$ mice. (**F**) Confocal microscopy of pLNs of *Spns2*$^{f/f}$ (left) and *Lyve1;Spns2*$^{\Delta/\Delta}$ (right) mice for CMTMR$^+$ BMDCs (red), PNAd$^+$ (green) HEVs and ERTR7$^+$ (blue) fibroblastic tissue networks. (**G**) Visualisation of the automated detection of individual CMTMR$^+$ BMDCs (white spheres) from PNAd$^+$ HEVs (green surface) in pLNs of *Spns2*$^{f/f}$ (left) and *Lyve1;Spns2*$^{\Delta/\Delta}$ (right) mice. Grey gradients visualise the distance transformation from HEVs (green surface) defined by PNAd-staining. (**H**) Total numbers of BMDCs (white spheres in (**F**)) in distances from 0 µm - 100 µm from HEVs counted in 10 µm radial areas around HEVs in pLNs of *Spns2*$^{f/f}$ and *Lyve1;Spns2*$^{\Delta/\Delta}$ mice. Each circle represents an individual mouse (**A, D**) or total numbers of BMDCs around HEVs in the visual field of a micrograph (**H**); bars indicate the mean. Scale bars, 5 µm (**C**), 50 µm (**B, F, G**). *p<0.05; **p<0.005; ***p<0.0005 (two-tailed unpaired Student's *t*-test (**A, D, H**)). Data are representative for six mice per group pooled from two (**A, B**) or three (**D**) independent experiments with n = 3 (**A**) or n = 4 per (**D**) mice group, for 2x pLNs and 2x iLNs of three mice per group (**C**), for 36x representative individual sections of 2x analyzed popliteal LNs per mouse pooled from two independent experiments (**H**) with n = 6 mice per group (**H**).

DOI: https://doi.org/10.7554/eLife.41239.007

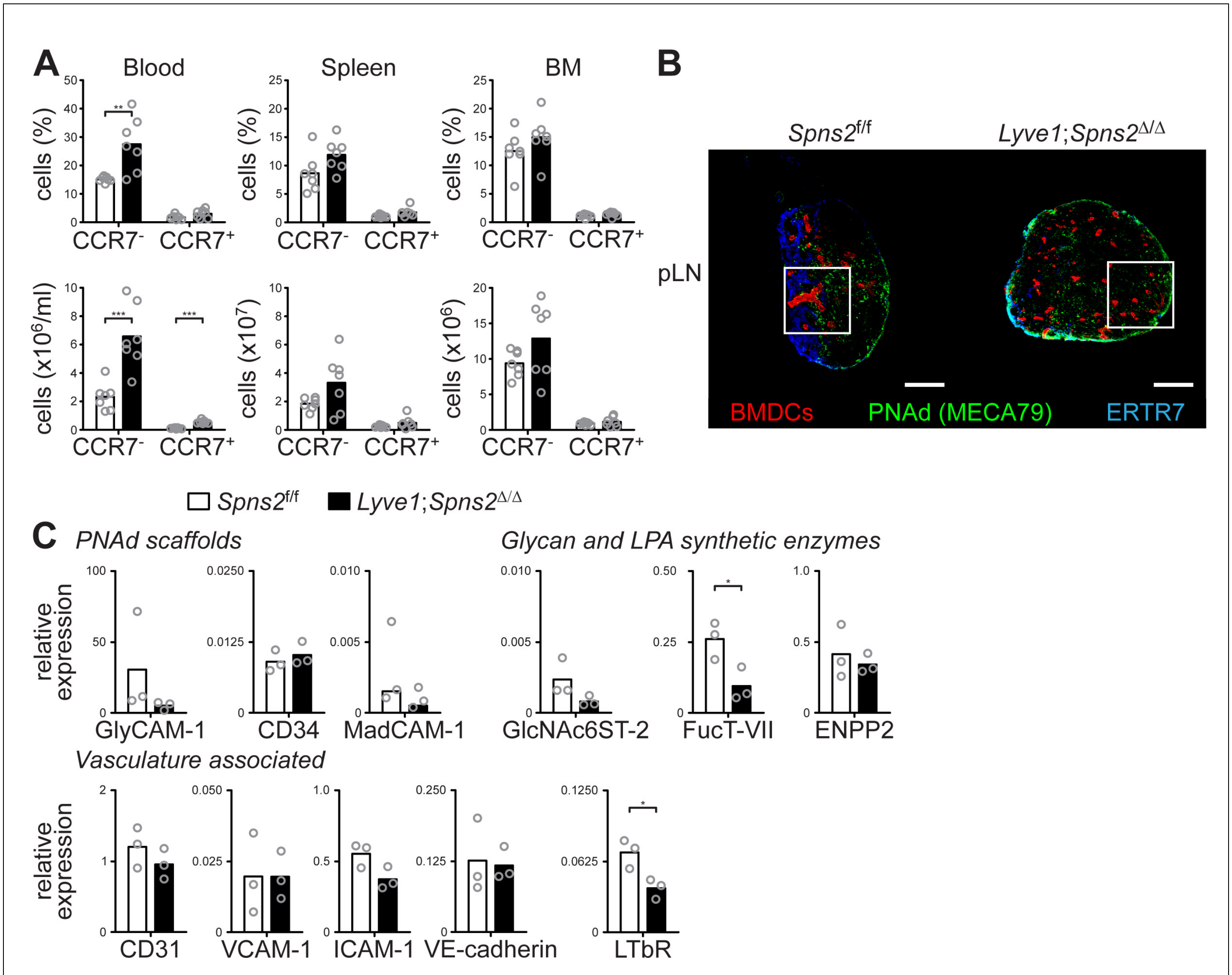

Figure 3—figure supplement 1. Endogenous DCs do not co-localize with HEVs in pLNs of Lyve1;*Spns2*$^{\Delta/\Delta}$ mice. (**A**) FACS analysis of CCR7$^-$ and CCR7$^+$ conventional mDCs (CD19$^-$/CD3$^-$/CD11c$^+$/MHC-II$^+$) in blood, spleen, and BM of *Spns2*$^{f/f}$ and *Lyve1;Spns2*$^{\Delta/\Delta}$ mice. (**B**) Confocal microscopy of pLNs of *Spns2*$^{f/f}$ (left) and *Lyve1;Spns2*$^{\Delta/\Delta}$ (right) mice for CD11c$^+$ (green) DCs, PNAd$^+$ (red) HEVs and Lyve-1$^+$ (blue) LECs. White squares show the regions of interest magnified and shown in ***Figure 3*** (**B**). (**C**) qRT-PCR analysis of the expression levels of PNAd scaffolds (GlyCAM-1, CD34, MadCAM-1), of Glycan and LPA synthetic enzymes (GlcNAc6ST-2, FucT-VII, ENPP2), and vascular associated genes (CD31, VCAM-1, ICAM-1, VE-cadherin, LTbR) in total mRNA isolated from CD45$^-$/CD31$^+$/PNAd$^+$ high-endothelial cells sorted from pLNs of *Spns2*$^{f/f}$ and *Lyve1;Spns2*$^{\Delta/\Delta}$ mice. Each circle (**A**) represents an individual mouse (**A**) or the relative chemokine expression levels in mRNA extracted from the total CD45$^-$/CD31$^+$/PNAd$^+$ high-endothelial cells (**C**); bars indicate the mean. Data are pooled from two independent experiments (**A**) with n = 3 or n = 4 mice per group (**A**), are representative for 18x individual sections of 2x analyzed pLNs, iLNs and bLNs per mouse pooled from three mice per group in two individual experiments (**B**), three independent mRNA preparations of 2x pLNs, iLNs and bLNs per mouse pooled from five mice per group (**C**), or seven (**D**) individual mice. Scale bars, 200 µm (**B**). *p<0.05; **p<0.005; ***p<0.0005 (two-tailed unpaired Student's *t*-test (**A, C**)).

DOI: https://doi.org/10.7554/eLife.41239.008

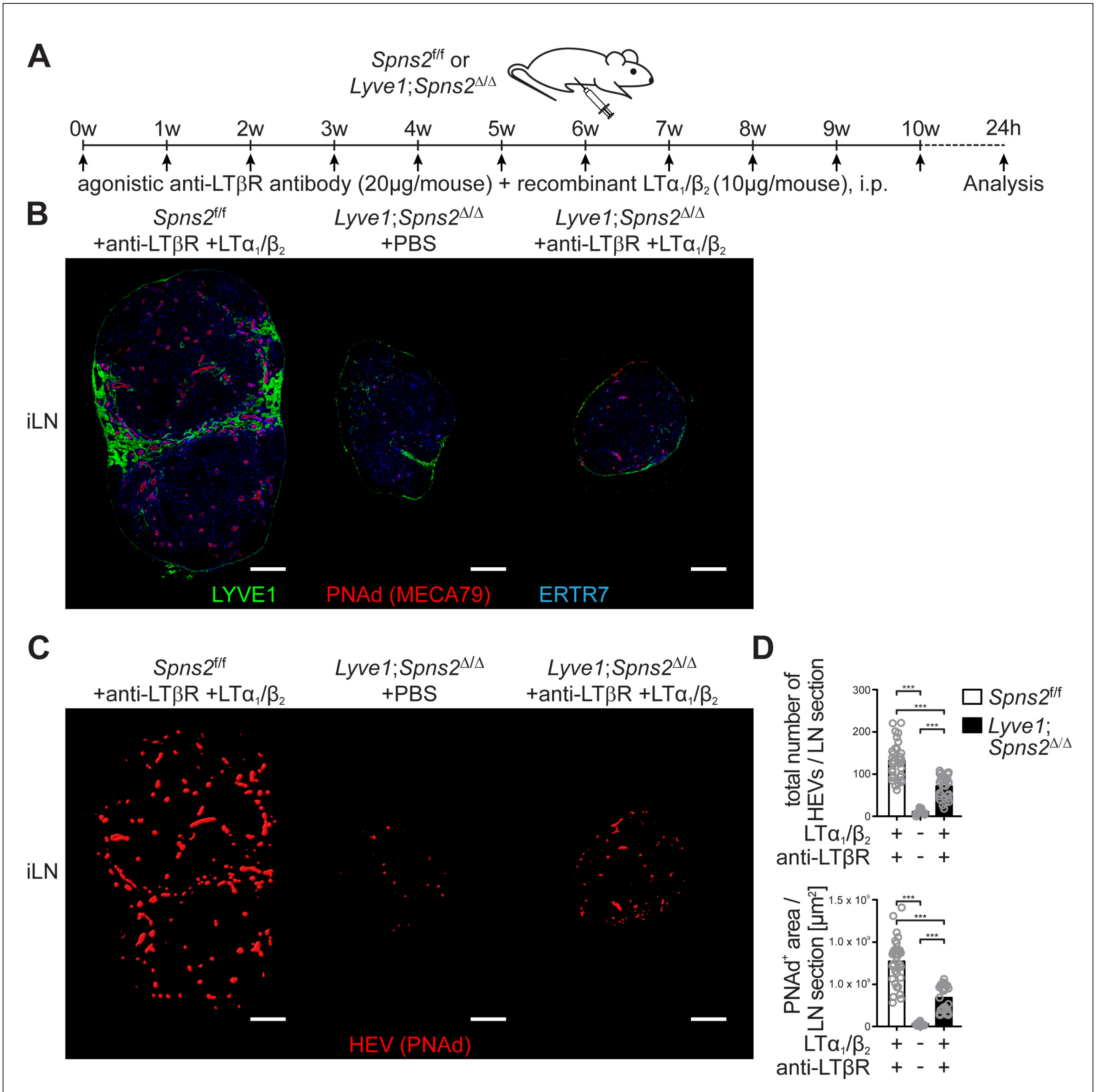

Figure 4. Combined anti-LTβr antibody and recombinant LTα1/β2 protein treatment partially rescues total high-endothelial cell numbers and HEV morphology. (**A**) Experimental flow-chart of PBS or agonistic anti-LTβr antibody (20 µg/mouse) and recombinant LTα1/β2 protein (10 µg/mouse) i.p. injections into *Spns2*$^{f/f}$ and *Lyve1;Spns2*$^{\Delta/\Delta}$ mice. (**B**) Confocal microscopy of iLNs of *Spns2*$^{f/f}$ mice +anti-LTβr antibody +LTα1/β2 (left), *Lyve1;Spns2*$^{\Delta/\Delta}$ mice +PBS (mid) and *Lyve1;Spns2*$^{\Delta/\Delta}$ mice +anti-LTβr antibody +LTα1/β2 (right) mice for LYVE1^{+} (green) LECs, PNAd^{+} (red) HEVs and ERTR7^{+} (blue) fibroblastic tissue networks. (**C**) Visualisation of the automated detection of PNAd^{+} HEVs (red surfaces) used for the quantification of the total numbers of HEVs/LN section and the total PNAd^{+} area/LN section of iLNs of *Spns2*$^{f/f}$ mice +anti-LTβr antibody +LTα1/β2 (left), *Lyve1;Spns2*$^{\Delta/\Delta}$ mice +PBS (mid) and *Lyve1;Spns2*$^{\Delta/\Delta}$ mice +anti-LTβr antibody +LTα1/β2 (right) mice. (**D**) The total numbers of HEVs/LN section and the total PNAd^{+} area/LN section extracted from the analyses shown in (**B**) and (**C**) of iLNs of *Spns2*$^{f/f}$ and *Lyve1;Spns2*$^{\Delta/\Delta}$ mice treated with +PBS or +anti-LTβr antibody +LTα1/β2. Each circle represents the total numbers of HEVs/LN section or the total PNAd^{+} area/LN section [µm^{2}] extracted from the micrographs (**B, C**), bars indicate

Figure 4 continued on next page

Figure 4 continued

the mean. Scale bars, 200 µm (**B, C**). ***p<0.0005 (two-tailed unpaired Student's *t*-test (**D**)). Data are shown for representative sections from 2x analyzed iLNs per mouse (**B, C**) selected from 21x – 33x individually analyzed sections of six mice per group (**D**).

DOI: https://doi.org/10.7554/eLife.41239.009

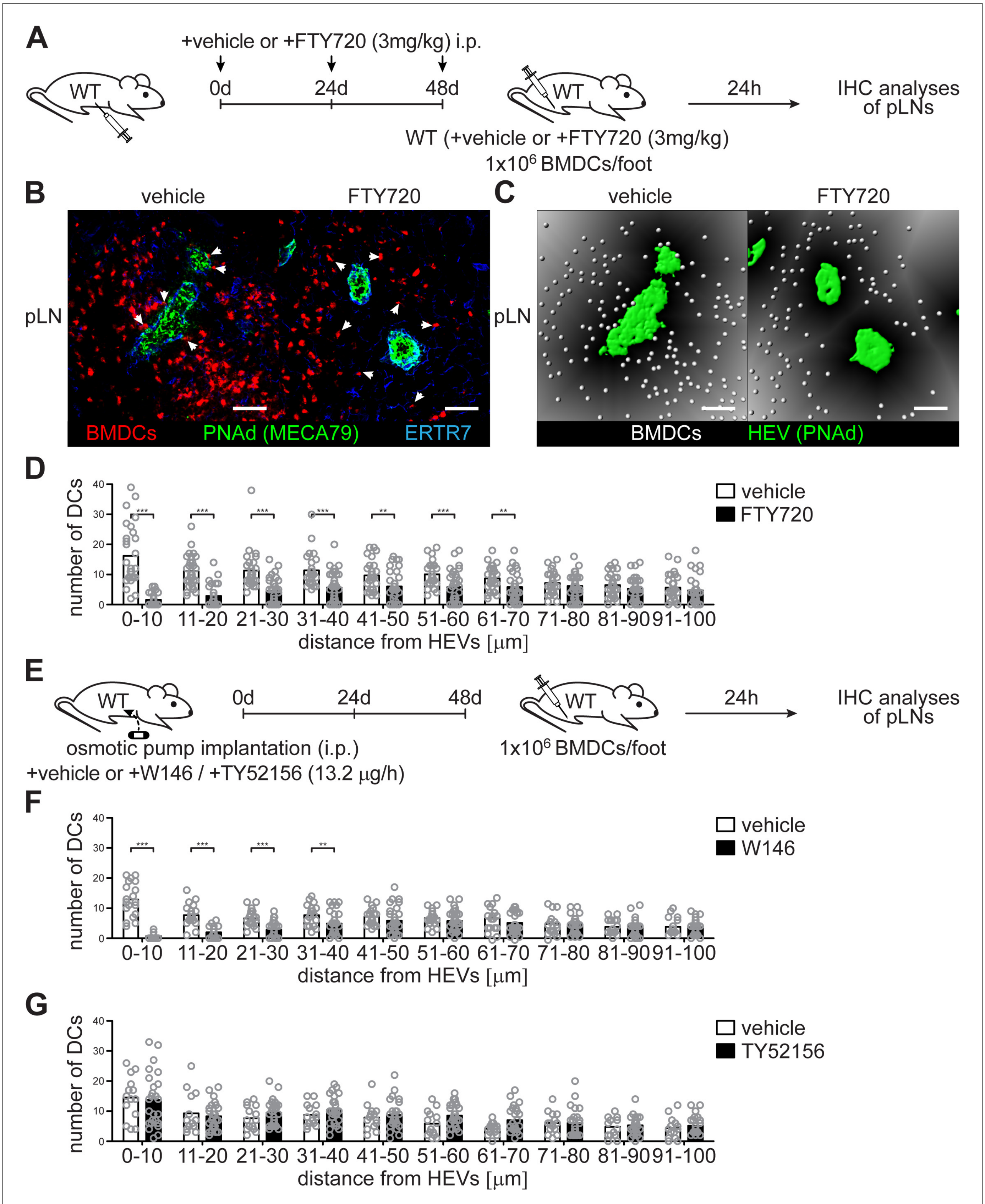
A
+vehicle or +FTY720 (3mg/kg) i.p.
WT
0d
24d
48d
WT
24h
IHC analyses of pLNs
WT (+vehicle or +FTY720 (3mg/kg)
1x10^6 BMDCs/foot
B
vehicle
FTY720
pLN
BMDCs
PNAd (MECA79)
ERTR7
C
vehicle
FTY720
pLN
BMDCs
HEV (PNAd)
D
number of DCs
vehicle
FTY720
0-10 11-20 21-30 31-40 41-50 51-60 61-70 71-80 81-90 91-100
distance from HEVs [μm]
E
WT
0d
24d
48d
WT
24h
IHC analyses of pLNs
osmotic pump implantation (i.p.)
+vehicle or +W146 / +TY52156 (13.2 μg/h)
1x10^6 BMDCs/foot
F
number of DCs
vehicle
W146
distance from HEVs [μm]
G
number of DCs
vehicle
TY52156
distance from HEVs [μm]

Figure 5. Co-localization of PNAd+ HEVs with lymph-derived BMDCs in pLNs is dependent on S1PR1- but not S1PR3-signalling. (**A**) Experimental flow-chart for the administration of the non-specific S1PR-antagonist FTY720 *i.p.* and lymphatic homing assays of footpad injected BMDCs to quantify HEV-DC interactions in pLNs in situ. (**B**) Confocal microscopy of pLNs of vehicle (left) or FTY720 (right) treated mice for CMTMR+ BMDCs (red), PNAd+ (green) HEVs and ERTR7+ (blue) fibroblastic tissue networks. (**C**) Visualisation of the distance of individual CMTMR+ BMDCs (white spheres) from PNAd+ HEVs (green surface) in pLNs of vehicle (left) or FTY720 (right) treated mice. Grey gradients visualise the distance transformation from HEVs (green surface) defined by PNAd-staining. (**D**) Total numbers of BMDCs (white spheres in (**B**)) in distances from 0 μm - 100 μm from HEVs (green surface in (**B**)) counted in 10 μm radial areas around HEVs in pLNs of vehicle or FTY720 treated mice. (**E**) Experimental flow-chart for the administration of the specific S1PR1-antagonist W146 and the S1PR3-antagonist TY52156, and lymphatic homing assays of BMDCs to quantify HEV-DC interactions in pLNs in situ. (**F, G**) Total numbers of BMDCs (white spheres as shown in (**C**)) in distances from 0 μm - 100 μm from HEVs counted in 10 μm radial areas around HEVs in pLNs of treated mice. Each circle represents the total numbers of BMDCs around HEVs in the visual field of a micrograph (**D, F, G**); bars indicate the mean. Scale bars, 50 μm (**B, C**). **$p<0.005$; ***$p<0.0005$ (two-tailed unpaired Student's *t*-test (**F, G**)). Data are representative for 37x representative individual sections of 2x analyzed popliteal LNs per mouse pooled from two independent experiments (**B, C, D**) with n = 6 mice per group (**B, C, D**) and for 34x (**F**) or 26x (**G**) representative individual sections of 2x analyzed popliteal LNs per mouse pooled from 5x mice per group (**F, G**).

DOI: https://doi.org/10.7554/eLife.41239.010

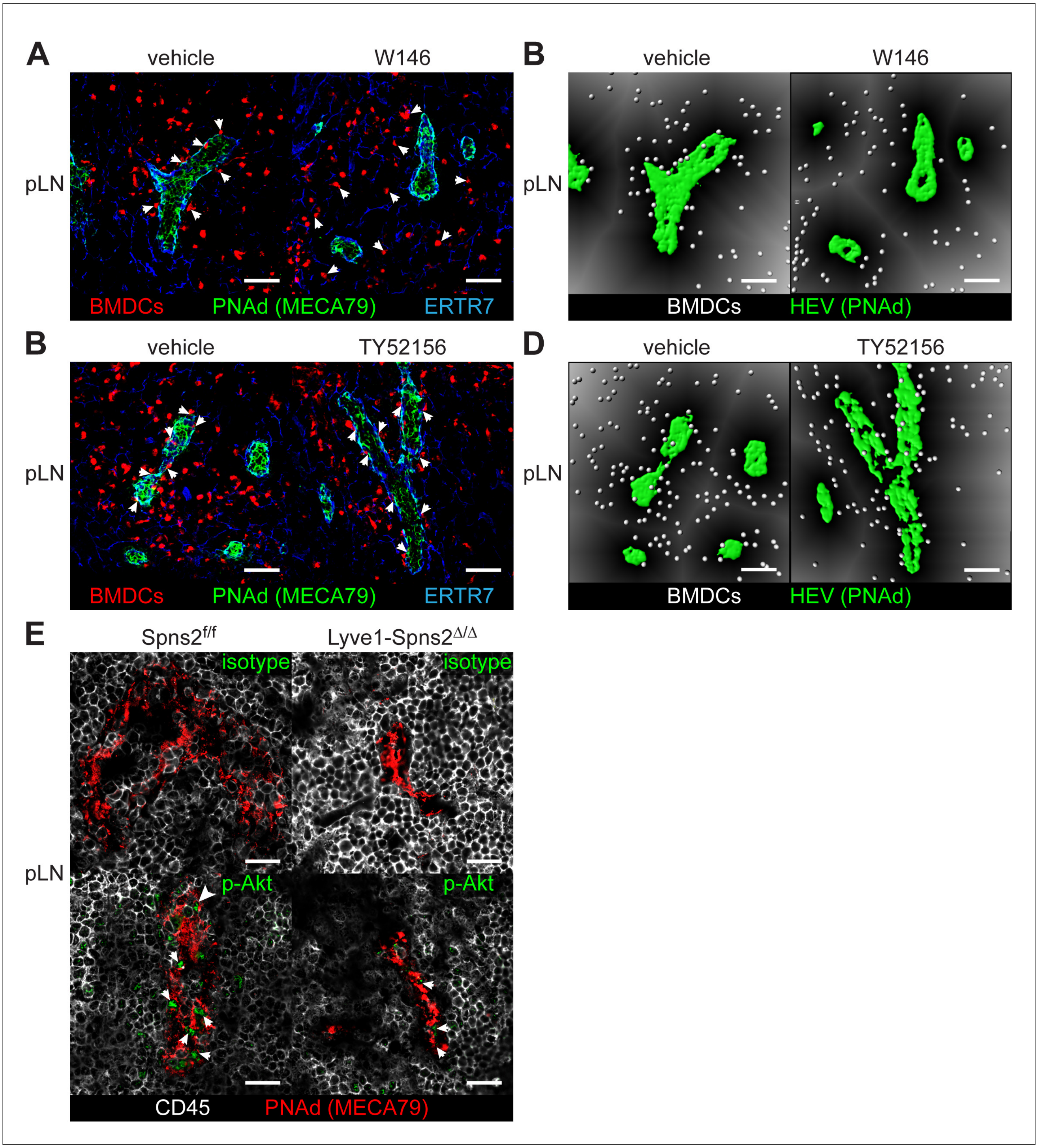

Figure 5—figure supplement 1. Co-localization of lymph-derived BMDCs with PNAd+ HEVs in pLNs is dependent on S1PR1- but not S1PR3-signaling. (**A**) Confocal microscopy of pLNs of vehicle (left) or W146 (right) treated mice for CMTMR+ BMDCs (red), PNAd+ (green) HEVs and ERTR7+ (blue) fibroblastic tissue networks. (**B**) Visualisation of the automated quantification of the distance of individual CMTMR+ BMDCs (white spheres) from PNAd+ HEVs (green surface) in pLNs of vehicle (left) or W146 (right) treated mice. Grey gradients visualise the distance transformation from HEVs (green

Figure 5—figure supplement 1 continued on next page

Figure 5—figure supplement 1 continued

surface) defined by PNAd-staining. (**C**) Confocal microscopy of pLNs of vehicle (left) or TY52156 (right) treated mice for CMTMR$^+$ BMDCs (red), PNAd$^+$ (green) HEVs and ERTR7$^+$ (blue) fibroblastic tissue networks. (**D**) Visualisation of the distance of individual CMTMR$^+$ BMDCs (white spheres) from PNAd$^+$ HEVs (green surface) in pLNs of vehicle (left) or TY52156 (right) treated mice. Grey gradients visualise the distance transformation from HEVs (green surface) defined by PNAd-staining. (**E**) Fluorescence microscopy of pLNs of *Spns2*$^{f/f}$ (left) and *Lyve1;Spns2*$^{\Delta/\Delta}$ (right) mice for isotype (top, green)/pAkt (bottom, green) on PNAd+ (red) HEVs and CD45+ (white) hematopoietic cells. Scale bars, 50 µm (**A–D**) and 20 µm (**E**). Data are representative for 2x analyzed popliteal LNs per mouse pooled from 5x mice per group (**A–D**), or are representative for five mice per group pooled from two independent experiments (**E**) with n = 2 or n = 3 mice per group (**E**).

DOI: https://doi.org/10.7554/eLife.41239.011

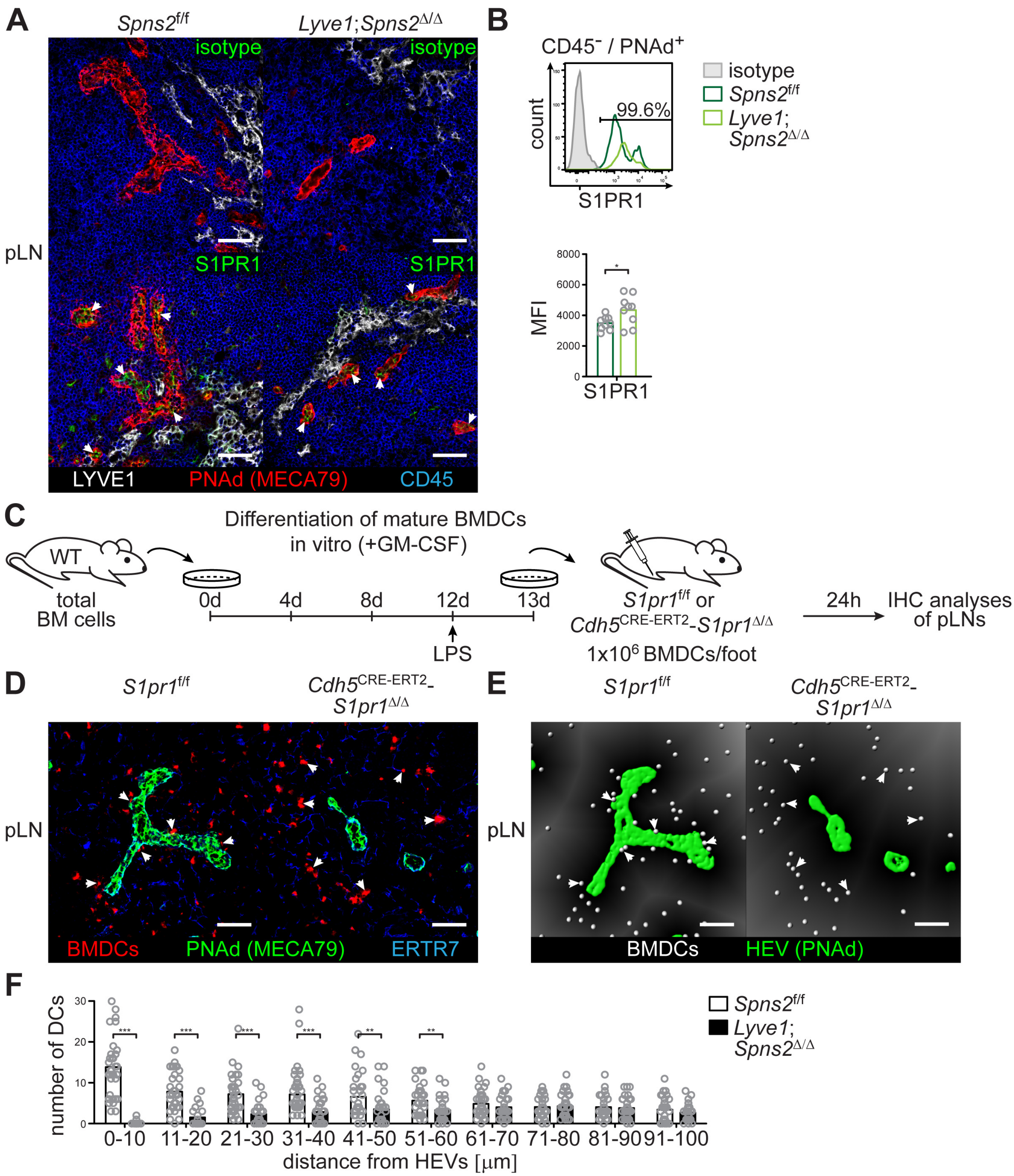

Figure 6. SPNS2-derived S1P controls autocrine S1PR1-G_i signalling in PNAd$^+$ HEVs of pLNs. (**A**) Fluorescence microscopy of pLNs of *Spns2*$^{f/f}$ (left) and *Lyve1;Spns2*$^{\Delta/\Delta}$ (right) mice for isotype (top, green)/S1PR1 (bottom, green) on PNAd$^+$ (red) HEVs and LYVE1$^+$ (white) LECs, and CD45$^+$ (blue)

Figure 6 continued on next page

Figure 6 continued

hematopoietic cells. (**B**) FACS analysis of the cell surface expression of S1PR1 on CD45$^-$/CD31$^+$/PNAd$^+$ high-endothelial cells in pLNs of *Spns2*$^{f/f}$ and *Lyve1;Spns2*$^{\Delta/\Delta}$ mice. (**C**) Experimental flow-chart of BMDC-differentiation in vitro, and lymphatic homing assays of footpad injected BMDCs to quantify DC-immigration from afferent lymphatics into pLNs of *S1pr1*$^{f/f}$ and *Cdh5*$^{CRE\text{-}ERT2}$;*S1pr1*$^{\Delta/\Delta}$ mice. (**D**) Confocal microscopy of pLNs of *S1pr1*$^{f/f}$ (left) and *Cdh5*$^{CRE\text{-}ERT2}$;*S1pr1*$^{\Delta/\Delta}$ (right) mice for CMTMR$^+$ BMDCs (red), PNAd$^+$ (green) HEVs and ERTR7$^+$ (blue) fibroblastic tissue networks. (**E**) Visualisation of the automated detection of individual CMTMR$^+$ BMDCs (white spheres) from PNAd$^+$ HEVs (green surface) in pLNs of *S1pr1*$^{f/f}$ (left) and *Cdh5*$^{CRE\text{-}ERT2}$;*S1pr1*$^{\Delta/\Delta}$ (right) mice. Grey gradients visualise the distance transformation from HEVs (green surface) defined by PNAd-staining. (**F**) Total numbers of BMDCs (white spheres in (**E**)) in distances from 0 μm - 100 μm from HEVs counted in 10 μm radial areas around HEVs in pLNs of *S1pr1*$^{f/f}$ and *Cdh5*$^{CRE\text{-}ERT2}$;*S1pr1*$^{\Delta/\Delta}$ mice. Each circle represents an individual mouse (**B**) or total numbers of BMDCs around HEVs in the visual field of a micrograph (**F**); bars indicate the mean. Scale bars, 50 μm (**A, D, G**). *p<0.05, **p<0.005; ***p<0.0005 (two-tailed unpaired Student's *t*-test (**B, F**)). Data are representative for five mice per group pooled from two independent experiments (**A**) with n = 2 or n = 3 mice per group (**A**), or are representative for nine mice per group pooled from three independent experiments (**B**) with n = 3 mice per group (**B**), or for 37x representative individual sections of 2x analyzed popliteal LNs per mouse pooled from two independent experiments (**F**) with n = 4 mice per group (**H**).

DOI: https://doi.org/10.7554/eLife.41239.012

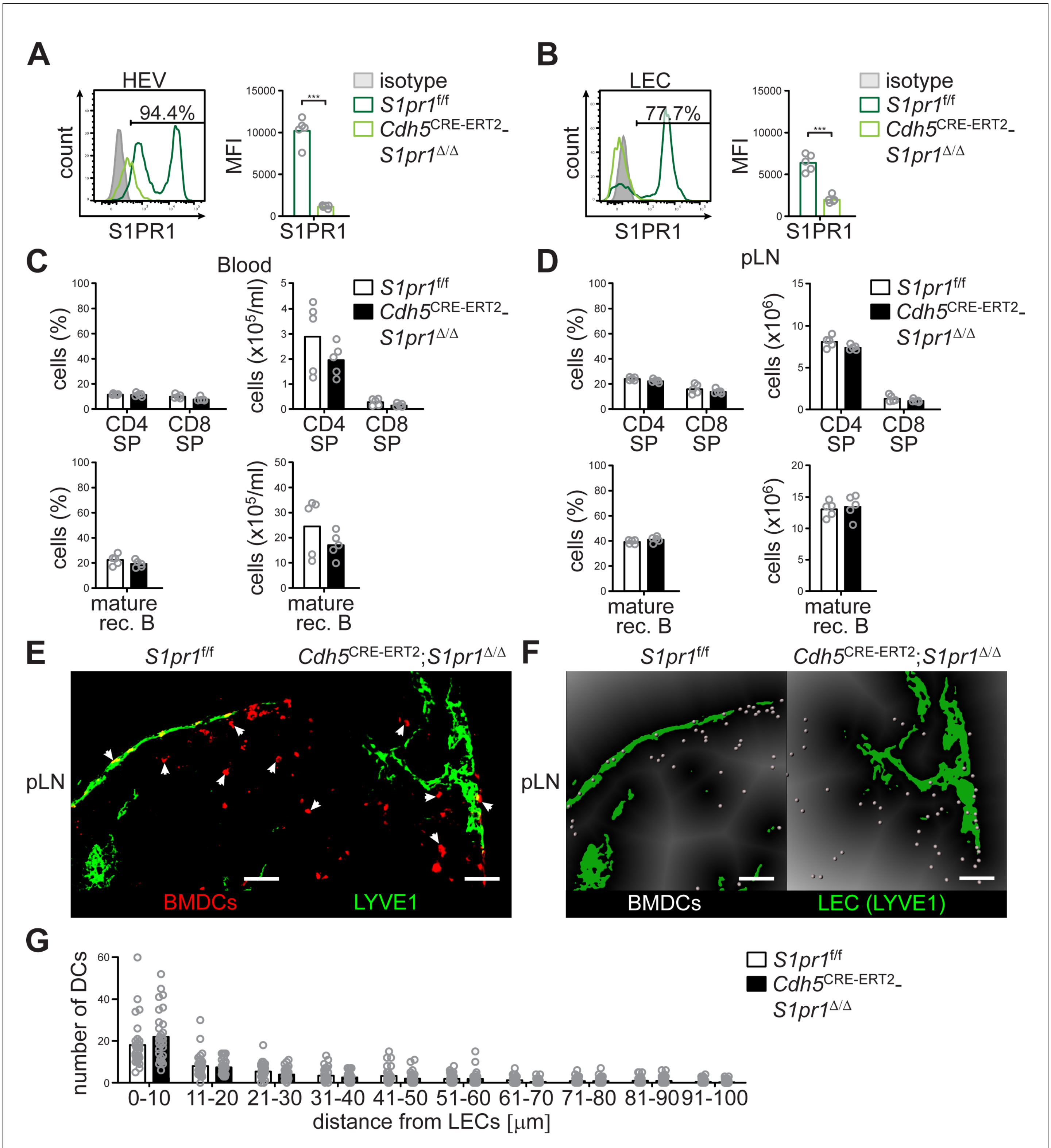

Figure 6—figure supplement 1. Endothelial-cell specific deletion of *S1pr1* does not affect lymphocyte immigration into pLNs, and does not influence DC-positioning at cortical lymphatics. (**A**) FACS analysis of the cell surface expression of S1PR1 on CD45$^-$/CD31$^+$/PNAd$^+$/LYVE1$^-$ high-endothelial cells and (**B**) on CD45$^-$/CD31$^+$/PNAd$^-$/LYVE1$^+$ LECs in pLNs of *S1pr1*$^{f/f}$ and *Cdh5*$^{CRE\text{-}ERT2}$;*S1pr1*$^{\Delta/\Delta}$ mice. (**C**) FACS analysis of CD4$^+$ and CD8$^+$ SP T-cells (top) and mature rec. B-cells (bottom) in the blood and (**D**) pLNs of *S1pr1*$^{f/f}$ and *Cdh5*$^{CRE\text{-}ERT2}$;*S1pr1*$^{\Delta/\Delta}$ mice. (**E**) Confocal microscopy of pLNs of S1pr1$^{f/f}$ and

Figure 6—figure supplement 1 continued on next page

Figure 6—figure supplement 1 continued

Cdh5$^{CRE-ERT2}$;*S1pr1*$^{\Delta/\Delta}$ mice for CMTMR^{+} BMDCs (red) and LYVE1^{+} (green) LECs. (**F**) Visualisation of the automated quantification of the distance of individual CMTMR^{+} BMDCs (white spheres) from LYVE1^{+} LECs (green surface) in pLNs of S1pr1$^{f/f}$ and *Cdh5*$^{CRE-ERT2}$;*S1pr1*$^{\Delta/\Delta}$ mice. Grey gradients visualise the distance transformation from LECs (green surface) defined by anti-LYVE1-staining. (**G**) Total numbers of BMDCs (white spheres in (**F**)) in distances from 0 μm - 100 μm from HEVs counted in 10 μm radial areas around LECs in pLNs of *S1pr1*$^{f/f}$ and *Cdh5*$^{CRE-ERT2}$;*S1pr1*$^{\Delta/\Delta}$ mice. Each circle represents an individual mouse (**A–D**) or total numbers of BMDCs around HEVs in the visual field of a micrograph (**G**); bars indicate the mean. Scale bars, 50 μm (**E–F**). *p<0.05, **p<0.005; ***p<0.0005 (two-tailed unpaired Student's *t*-test (**A–D, G**)). Data are representative for five mice per group pooled from two independent experiments (**A–D**) with n = 2 or n = 3 mice per group (**A–D**), or for 29x representative individual sections of 2x analyzed popliteal LNs per mouse pooled from two independent experiments (**E–F**) with n = 4 mice per group (**G**).

DOI: https://doi.org/10.7554/eLife.41239.013

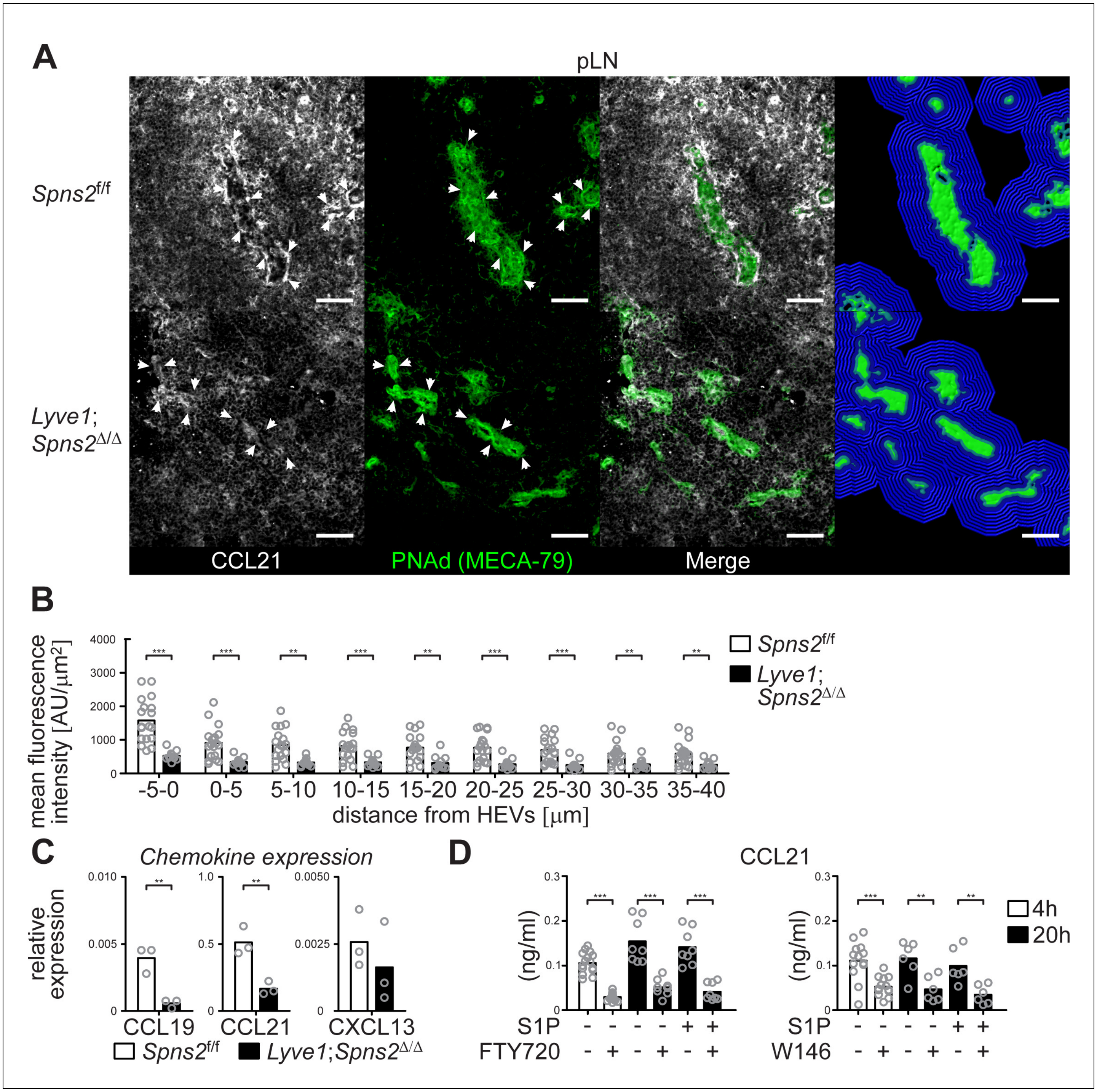

Figure 7. CCL21-production and -release from HEVs is severely impaired in pLNs of *Lyve1;Spns2*$^{\Delta/\Delta}$ mice. (**A**) The IHC analysis of CCL21 (white) distribution around PNAd^{+} HEVs, and visualisation of the automated detection of PNAd^{+} HEVs (green surface) and of the radial areas (blue) around HEVs used for the quantification of the mean fluorescent intensity of the CCL21 signal in pLNs of in *Spns2*$^{f/f}$ (top) and *Lyve1;Spns2*$^{\Delta/\Delta}$ (bottom) mice. (**B**) The mean fluorescent intensity of the CCL21 signal in distances from −5 μm to 40 μm from the outer border of HEVs (green surface in (**C**)) determined in 5 μm radial areas around HEVs in pLNs of *Spns2*$^{f/f}$ and *Lyve1;Spns2*$^{\Delta/\Delta}$ mice. (**C**) qRT-PCR analysis of CCL19, CCL21 and CXCL13 expression levels in total mRNA isolated from CD45^{-}/CD31^{+}/PNAd^{+} high-endothelial cells sorted from pLNs of *Spns2*$^{f/f}$ and *Lyve1;Spns2*$^{\Delta/\Delta}$ mice. (**D**) ELISA of the CCL21 levels of the supernatant of high-endothelial cells cultivated with or without 10 μM FTY720 (left) or 10 μM W146 (right) in vitro. Each circle represents the mean fluorescent intensity of the CCL21 signal detected around HEVs in the visual field of a micrograph (**B**), the relative chemokine expression levels in mRNA extracted from the total CD45^{-}/CD31^{+}/PNAd^{+} high-endothelial cells (**C**), or the CCL21 protein levels detected in the supernatant of individual cell cultures (**D**) of CD45^{-}/CD31^{+}/PNAd^{+} high-endothelial cells; bars indicate the mean. Scale bars, 50 μm (**A**). $^{**}p<0.005$; $^{***}p<0.0005$ (two-tailed

Figure 7 continued on next page

Figure 7 continued

unpaired Student's *t*-test (**B–D**)). Data are representative for 18x individual sections of 2x analyzed pLNs, iLNs and bLNs per mouse pooled from three mice per group (**A, B**), three independent mRNA preparations of 2x pLNs, iLNs and bLNs per mouse pooled from five mice per group (**C**), or three independent stimulations with n = 2 to n = 4 of a total of 8x – 16x (FTY720) or 6x – 12x (W146) individual cell cultures (**D**) with total sorted high-endothelial cells from 2x pLNs, iLNs and bLNs per mouse pooled from five mice per group in vitro.

DOI: https://doi.org/10.7554/eLife.41239.014